MATERIALS SCIENCE

Translational and rotational critical-like behaviors in the glass transition of colloidal ellipsoid monolayers

Zhongyu Zheng[1,2], Ran Ni[3], Yuren Wang[1,2]*, Yilong Han[4]*

Critical-like behaviors have been found in translational degrees of freedom near the glass transition of spherical particle systems mainly with local polycrystalline structures, but it is not clear if criticality exists in more general glassy systems composed of nonspherical particles without crystalline structures. Here, through experiments and simulations, we show critical-like behaviors in both translational and rotational degrees of freedom in monolayers of monodisperse colloidal ellipsoids in the absence of crystalline orders. We find rich features of the Ising-like criticality in structure and slow dynamics at the ideal glass transition point ϕ_0, showing the thermodynamic nature of glass transition at ϕ_0. A dynamic criticality is found at the mode-coupling critical point ϕ_c for the fast-moving clusters whose critical exponents increase linearly with fragility, reflecting a dynamic glass transition. These results cast light on the glass transition and explain the mystery that the dynamic correlation lengths diverge at two different temperatures.

INTRODUCTION

The nature of the glass transition is a major puzzle in condensed matter physics. There are many competing theories explaining some of the behaviors of the glass transition (*1*), but the fundamental picture remains controversial, e.g., whether the glass transition is a pure dynamic transition or a thermodynamic transition. The thermodynamic origin of the glassy dynamics is pursued in various theories such as the Adam-Gibbs theory (*2*), random first-order transition (RFOT) theory (*3*), frustration-limited domain theory (*4*), and the potential landscape approach (*5*). However, these theories do not provide enough quantitative predictions for experimental verification, resulting in controversies over the thermodynamic nature of the glass transition.

Intensive efforts have been made to reveal the structural features of the dynamic slowdown as evidence of the thermodynamic nature of the glass transition. The drastic dynamic slowdown near the glass transition is usually accompanied by the growth of dynamic heterogeneities (DHs) arising from cooperatively rearranging regions (CRRs) at different time scales (*1*, *6*–*11*). The intuitive picture of CRRs is thermodynamically rationalized in various theories (*2*–*5*, *12*) and is intimately associated with the physical, chemical, and mechanical properties of glassy materials (*5*, *10*, *13*, *14*). Generally, two approaches may be used to uncover the structural mechanism underlying the glass transition. One approach is to find a certain local structure associated with fast- or slow-moving particles, e.g., an icosahedron (*14*), a tetrahedron (*15*), a crystalline structure (*16*–*20*), a low-entropy structure (*18*, *21*), or an empirical structure from machine learning (*22*). Related studies have been focused on spherical particle systems, but apparently, polyhedra and crystallites usually do not exist in nonspherical particle systems. Besides controversy over which candidate structure is responsible for the slow dynamics, the observed spatial structure-dynamics correlations alone cannot unequivocally prove the structural origin of slow dynamics, because correlation does not imply causation. The second approach is the order-agnostic method, which searches for a growing static length scale upon cooling toward the glass transition (*1*, *7*, *23*, *24*). This approach lacks a correlation to dynamic quantities and a corresponding structure for the order-agnostic length (*25*, *26*); thus, it is less direct than the first approach.

Besides the above two approaches, stronger evidence of thermodynamic transition has been obtained from the Ising-like critical behaviors in two-dimensional (2D) and 3D polydisperse colloidal spheres, 3D Lennard-Jones liquids, 2D and 3D binary soft spheres, 2D driven granular spheres, 2D spin liquids with anisotropic attractions, and 3D polydisperse Lennard-Jones liquids with isotropic attraction (*17*–*20*, *27*). Critical phenomena are well understood in physics with many quantitative predictions that can be experimentally tested (*28*, *29*), in contrast to glass transition theories. These critical-like behaviors are mainly found in local crystalline clusters (*17*–*20*) or low–structural entropy clusters in systems of spheres, leading to the question of whether the Ising criticality only occurs in certain spherical particle systems (*26*). Most glasses are not composed of spherical particles. Whether the Ising criticality exists in more general glassy systems composed of nonspherical particles or in rotational degrees of freedom has not been explored. Here, we show both Ising-like criticality and non-Ising criticality in glassy monolayers of ellipsoids.

Monodisperse hard ellipsoids are one of the simplest glass formers. In contrast to spheres, colloidal ellipsoids have measurable rotational motions and can form 2D glasses without the crystalline or polyhedral order observed in spherical particle systems (*30*). Thus, they are excellent models to study the general relationship between static structures and glassy dynamics and the existence of criticality. Previously, we showed the substantial effects of particle aspect ratio $p = a/b$ on the glass transition, where a and b are the semi-long and semi-short axes of ellipsoid's (*30*, *31*). The phase behavior of hard ellipsoids depends on both the area fraction ϕ and p. The inverse of area fraction ϕ^{-1} plays the role of effective temperature T (see section S2 for the possible phases of monodisperse hard ellipsoids). The glass transition of the translational (T) and rotational (θ) motions of the monolayer of colloidal hard ellipsoids occurs in a single step at $p \lesssim 2.5$, i.e., $\phi_c^T = \phi_c^\theta$ for the mode-coupling theory (MCT) transition and $\phi_0^T = \phi_0^\theta$ for the ideal glass transition, but in two steps at $p \gtrsim 2.5$, i.e., $\phi_c^\theta < \phi_c^T$ and $\phi_0^\theta < \phi_0^T$ as shown in figs. S1 and S2. We also found the structural signatures of both translational and rotational

[1]Institute of Mechanics, Chinese Academy of Sciences, Beijing, China. [2]School of Engineering Science, University of Chinese Academy of Sciences, Beijing, China. [3]School of Chemical and Biomedical Engineering, Nanyang Technological University, Singapore. [4]Department of Physics, The Hong Kong University of Science and Technology, Hong Kong, China.
*Corresponding author. Email: yilong@ust.hk (Y.H.); yurenwang@imech.ac.cn (Y.W.)

DHs in the single-step and two-step glass transitions in (*30*). The increasing dynamic slowdown and growing DHs upon cooling were correlated with a decreasing structural entropy and a growing size typically used in the literature to demonstrate the thermodynamic nature of the glass transition.

In this study, we show rich critical-like behaviors and correlations for various structural and dynamic quantities in both translational and rotational motions of ellipsoids as summarized in Table 1. We find Ising-like criticality in both the local structural quantities and the slow-moving clusters at ϕ_0, indicating a thermodynamic transition at ϕ_0, whereas the fast-moving clusters show a criticality at ϕ_c without a structural counterpart, indicating a dynamic transition at ϕ_c. These results are further confirmed by our kinetic Monte Carlo (kMC) simulations.

RESULTS

Correlations among dynamic and structural heterogeneities

A key mystery of the glass transition is the drastic dynamic slowdown without obvious structural change upon cooling. Whether DHs or CRRs arise from structural heterogeneities is crucial for the nature of the glass transition and one of the main challenges in glass studies (*1*, *5*). Searching for a certain local structure associated with CRRs is a major direction in glass studies. CRRs have been intensively studied in glasses composed of spherical particles (*1*, *6*–*10*) and related to various symmetric structures in simulations (*1*, *7*, *14*, *16*, *18*, *20*, *22*, *23*, *27*) and experiments (*15*, *17*, *21*), but CRRs in anisotropic particles remain poorly understood.

We characterize the local dynamics using not only the conventional fastest-translation (FT) and fastest-rotation (FR) particles but also the much less explored slowest-translation (ST) and slowest-rotation (SR) particles (section S3) (*30*). These four types of particles have displacements that deviate from Gaussian distributions, and each makes up ~8 to 10% of all particles and forms clusters in supercooled liquids, reflecting the DHs (Fig. 1, A to H). The time interval in the definition of fast or slow particles is chosen as when the average cluster size $\langle N\rangle$ reaches the maximum. This time interval is proportional to τ_2 for the fast clusters (*9*, *30*) and to τ_4 for the slow clusters (*6*, *18*, *30*). τ_2 corresponds to the maximal non-Gaussian parameter α_2 of the particles' displacements; τ_4 corresponds to the maximal four-point correlation length ξ_4, which is on the same order as the structural relaxation time τ_α. Details of α_2 and ξ_4 are presented in section S3.

It is well known that the liquid-to-glass transition does not exhibit obvious density fluctuations, in contrast to the traditional liquid-gas transition at the critical point. Thus, density is not an appropriate order parameter for the study of critical-like behaviors in glasses, and other structural order parameters are needed. Here, we characterize the local structure of each individual particle by the translational and orientational glassy orders $\psi_G^{T,\theta}$, as well as the translational and orientational structural entropies $\psi_S^{T,\theta}$ as defined in Table 1 and sections S4 and S5. The translational glassy (GT) particles are defined as those with the number of nearest neighbors $\psi_G^T \geq 6$ because the mean coordination number is about 6 near the maximally random-jammed packing of ellipses in 2D (*32*). We find that having more neighbors can restrict the translational motion more strongly, but not the rotational motion at $p \gtrsim 2.5$, especially for particles lying on the boundaries of quasi-nematic domains (Fig. 1, C and D). The rotational glassy (GR), i.e., orientational glassy, particles are defined as those with $\psi_G^\theta \geq 0.8$ because a local nematic structure suppresses rotation (*30*). These glassy particles form clusters in supercooled liquids (Fig. 1, A to H), reflecting the structural heterogeneities.

We find that the structural heterogeneities and DHs are correlated differently at $p \lesssim 2.5$ and $p \gtrsim 2.5$ (table S1 and fig. S3) because ellipsoids

Table 1. Critical-like behaviors near ϕ_0 and ϕ_c in the monolayers of colloidal ellipsoids.

	Dynamic criticality		Structural criticality		
Dynamic and structural quantities	Fast cluster (ψ = FT, FR) ~8–10% fastest-moving particles	Slow cluster (ψ = ST, SR) ~8–10% slowest-moving particles	Glassy cluster (ψ = GT, GR) GT particles: $\psi_G^T \geq 6$ GR particles: $\psi_G^\theta \geq 0.8$	Glassy order (ψ_G^T, ψ_G^θ) ψ_G^T: Number of nearest neighbors $\psi_{Gi}^\theta = \sum_{j=1}^{\psi_G^T} \cos(2\Delta\theta_{ij})/\psi_G^T$	Structural entropy (ψ_S^T, ψ_S^θ) $\psi_{Si}^T = -\pi k_B \rho \int_0^\infty [g_i(r)\ln g_i(r) - g_i(r) + 1]dr$ $\psi_{Si}^\theta = -\frac{1}{2} k_B \rho \int_0^\infty g_i(r)dr \int_0^{2\pi} g_i(\theta\|r)\ln[g_i(\theta\|r)]d\theta$
Critical-like behaviors	Mean diameter of the cluster	$\xi_\psi = \langle N_\psi \rangle^{1/d_f} \propto [\phi/(\phi_{c,0} - \phi)]^\nu$ (Figs. 2d,f, S5d,f) (Figs. 2a,c, S5a,c) (Figs. S3a, S6a)	Spatial correlation	$C(r = \lvert r_i - r_j \rvert) = \langle \psi_i(r_i)\psi_j(r_j) \rangle = r^{-\eta} \exp(-r/\xi_\psi)$ (Figs. 3a-d, S7a-d)	
			Finite-size scaling	$\xi_\psi(L,\phi), \chi_\psi(L,\phi) \sim L^{\gamma/\nu} Q_{\xi,\chi}(L^{1/\nu}(1/\phi - 1/\phi_0))$ (Figs. 3e-h, S7e-h)	
	Cluster size fluctuation	$\chi_\psi = \langle N_\psi^2 \rangle / \langle N_\psi \rangle \propto [\phi/(\phi_{c,0} - \phi)]^\gamma$ (Figs. 2e,f, S5e,f) (Figs. 2b,c, S5b,c) (Figs. S3b, S6b)	Correlation length	$\xi_\psi \propto [\phi/(\phi_0 - \phi)]^\nu$ (Figs. 4a,d,c,f, S8a,d,c,f)	
			Susceptibility	$\chi_\psi = \langle \lvert \sum \psi_i(r_i) \rvert^2 \rangle / (N\rho) \propto [\phi/(\phi_0 - \phi)]^\gamma$ (Figs. 4b,e,c,f, S8b,e,c,f)	
	Cluster size distribution	$P(N_\psi) \sim N_\psi^{-\mu} \exp(-N_\psi/N_{\psi 0})$ (Figs. 1j, S4j)	Dynamic correlation	$S_\psi(q,t) = \langle \psi(-q,0)\psi(q,t) \rangle / (N\rho) = \chi_q \exp(-t/\tau_q)$ (Figs. 5a,b)	
			Lifetime	$\tau(q,\phi) \propto [\phi/(\phi_0 - \phi)]^\gamma / [1 + (q\xi_\psi)^{2-\eta}]$ (Figs. 5c,d)	
	Hyperscaling relation	$\gamma = 2\nu(d_f - 1), \mu = 2/d_f + 1$ (Figs. 1i,j, S4i,j)	Fisher scaling law	$\gamma = \nu(2 - \eta)$	
	$1/\phi$: Effective temperature; D: Fragility index; $\psi(q,t) = \sum_i \psi_i e^{iq \cdot r_i}$; N: Particle number; ρ: Particle density				
Critical exponent	$\nu, \gamma \propto 1/D$	$\nu = 1, \quad \gamma = 7/4, \quad \eta = 1/4$ (2D Ising)			
Critical point	ϕ_c: Mode-coupling point	ϕ_0: Ideal glass transition point			
Summary	One-step glass transition at $p \lesssim 2.5$ (simulation $p \lesssim 1.7$) Criticality of FT and FR clusters ($\phi_c^T = \phi_c^\theta$) Criticality of ST and SR clusters; GT clusters, ψ_G^T, and ψ_S^T ($\phi_0^T = \phi_0^\theta$)		Two-step glass transition at $p \gtrsim 2.5$ (simulation $p \gtrsim 1.7$) Criticality of FR clusters (ϕ_0^θ) Criticality of FT clusters (ϕ_0^T) Criticality of SR clusters, GR clusters, ψ_G^θ, and ψ_S^θ (ϕ_0^θ) Criticality of SR clusters, GT clusters, ψ_G^T, and ψ_S^T (ϕ_0^T)		

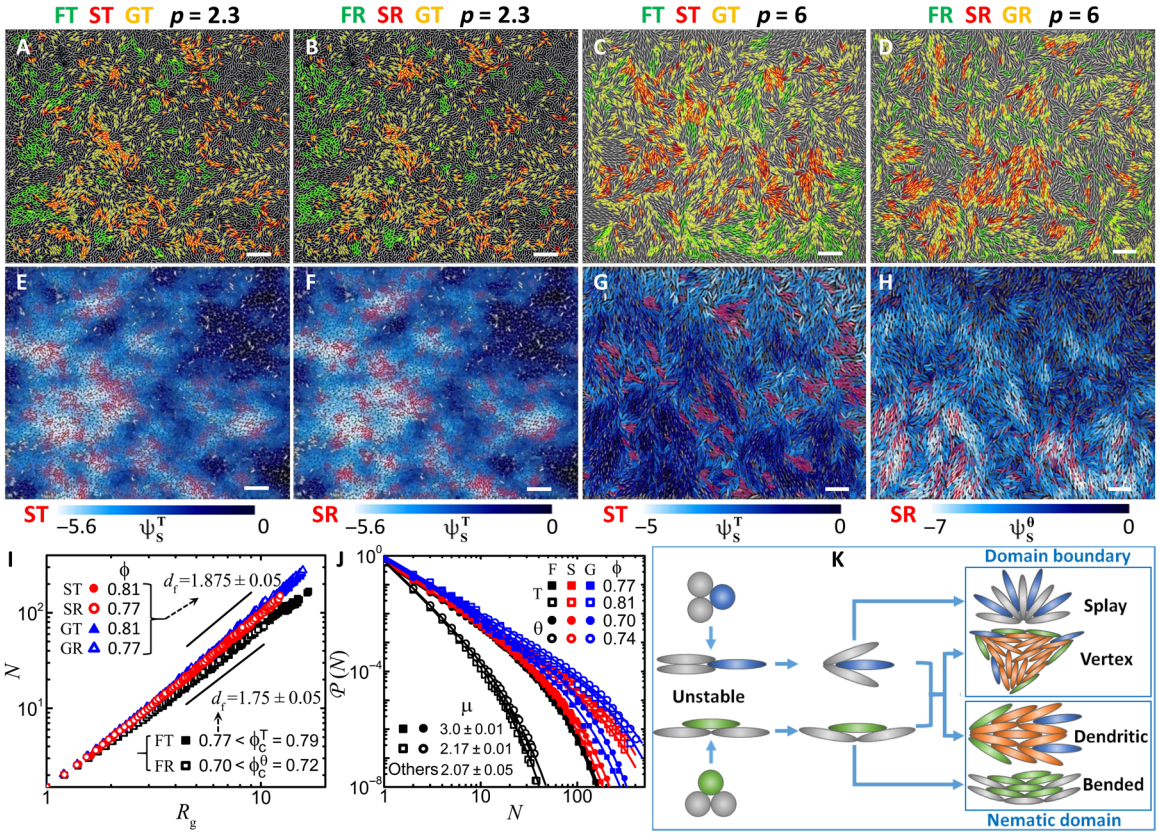

Fig. 1. Properties and spatial correlations between fast (F), slow (S), and glassy (G) clusters and structural entropy ψ_S in translational (T) and rotational (R) motions. (**A** to **H**) Fast (~8%), slow (~8%), and glassy (~30%) particles are shown in green, red, and yellow, respectively. The same video frame in (A) and (B) or (E) and (F) at $\phi = 0.81$ for $p = 2.3$, and in (C) and (D) or (G) and (H) at $\phi = 0.74$ for $p = 6$. (A and E) ST and (B and F) SR clusters are positively correlated with (A and B) GT clusters and (E and F) low ψ_S^T regions. (C and G) ST and (D and H) SR clusters are positively correlated with (C) GT and (D) GR clusters, and (G) low ψ_S^T and (H) low ψ_S^θ regions. Translational and rotational motions in (C) and (D) are negatively correlated. Scale bars, 20 μm. (**I**) The cluster size fitted with $N \propto R_g^{d_f}$, where R_g is the radius of gyration. (**J**) The probability distribution of cluster sizes (symbols) fitted with $\mathcal{P}(N) \sim N^{-\mu} \exp(-N/N_0)$ (curves). $p = 6$ in (I) and (J). The SD of each data point calculated from different clusters or frames is smaller than the symbol size. (**K**) Locally favored close packing configurations.

are randomly oriented at $p \lesssim 2.5$ and form quasi-nematic domains at $p \gtrsim 2.5$ (Fig. 1). For $p \gtrsim 2.5$, ST clusters are correlated with the regions of high ψ_G^T (Fig. 1C) and low ψ_S^T (Fig. 1G) at the boundaries of quasi-nematic domains, while SR clusters are correlated with the regions of high orientational glassy order ψ_G^θ (Fig. 1D) and low orientational structural entropy ψ_S^θ (Fig. 1H) within domains, i.e., SR clusters are anticorrelated with ST clusters. By contrast, for $p \lesssim 2.5$, both ST and SR clusters are strongly correlated with the regions of high GT order ψ_G^T (Fig. 1, A and B) and low translational structural entropy ψ_S^T (Fig. 1, E and F). Note that GR particles are not colored in Fig. 1B because small-p ellipsoids do not form quasi-nematic domains and do not have GR clusters. Hence, translational and rotational motions vitrify at the same glass transition density at $p \lesssim 2.5$ but at different densities at $p \gtrsim 2.5$.

Critical-like behaviors in dynamic FT, FR, ST, and SR clusters

Despite their different spatial distributions and correlations as described above, the translational and rotational DHs in the single-step and two-step glass transitions exhibit significant common features: the non-Ising critical-like behaviors of the fast CRRs near ϕ_c and the Ising-like critical behaviors of the slow clusters near ϕ_0. We find that the mean cluster diameter $\xi_{F,S} \equiv [\Sigma N_{F,S}\mathcal{P}(N_{F,S})]^{1/d_f} \propto [\phi/(\phi_{c,0} - \phi)]^{\nu}$, and the fluctuations in cluster size, i.e., susceptibility, $\chi_{F,S} \equiv \Sigma N^2\mathcal{P}(N)/\Sigma N\mathcal{P}(N) \propto [\phi/(\phi_{c,0} - \phi)]^{\gamma}$ on approaching $\phi_c^{T,\theta}$ for the FT and FR clusters and $\phi_0^{T,\theta}$ for the ST and SR clusters at all aspect ratios (Fig. 2 and Table 1). $N_{F,S}$ is the number of particles in a fast- or slow-moving cluster. d_f is the fitted fractal dimension (Fig. 1I), and $\mathcal{P}(N)$ is the size distribution of the clusters (Fig. 1J). For ST and SR clusters, ξ_S and χ_S at different p's collapse onto two power laws (Fig. 2, A to C) with exponents $\nu = 1$ and $\gamma = 7/4$ within ±5% errors, respectively, agreeing with the critical exponents belonging to the 2D Ising universality class (*29*). For fast particles, ξ and χ increase on approaching ϕ_c with non-Ising exponents, but drop precipitously (Fig. 2, D and E) at $\phi > \phi_c$ because the fast particles disperse randomly without forming clusters (Fig. 1D). By contrast, $\xi(\phi)$ and $\chi(\phi)$ of slow particles increase monotonically across ϕ_c (Fig. 2, A and B).

We measure the translational and rotational relaxation times τ_α^T and τ_α^θ from the decay of the intermediate scattering functions and the angular correlation functions, respectively (fig. S2, A and B) (*31*). τ_α can be well fitted by the Vogel-Fulcher-Tammann (VFT) law $\tau_\alpha \propto \exp[D(\phi_0^{-1})/(\phi^{-1} - \phi_0^{-1})]$ (fig. S2D) (*5*, *30*), where D is the fragility index. A higher D represents lower fragility, i.e., a stronger structural frustration against crystallization (*20*). Which factors affect

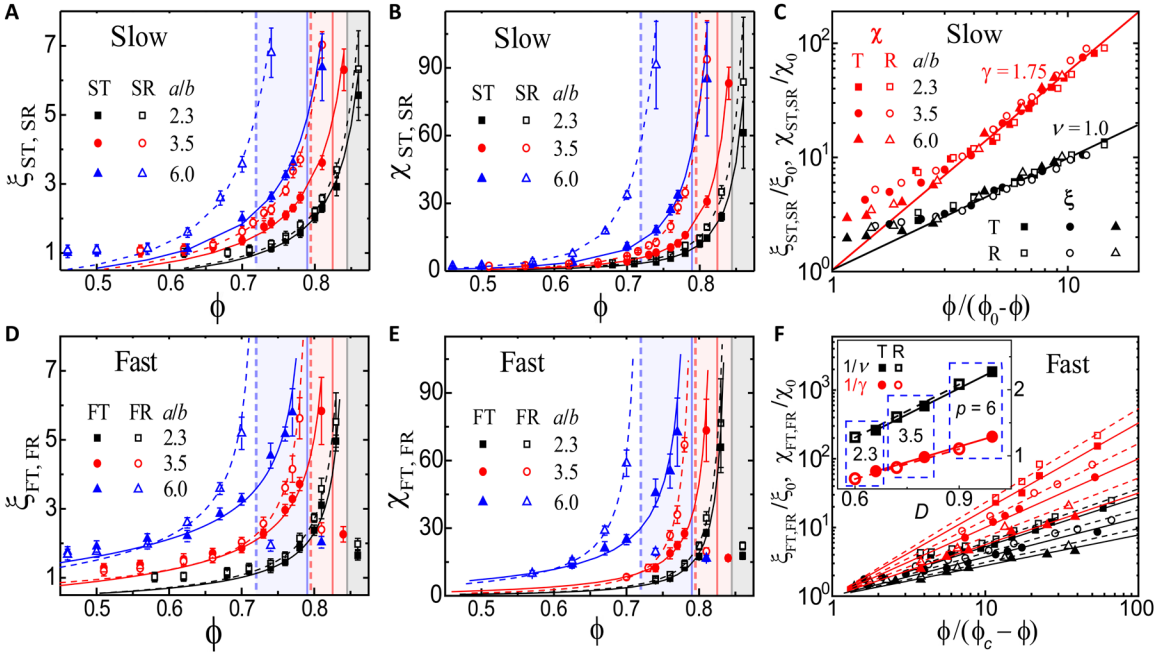

Fig. 2. Critical-like behaviors of the dynamic CRRs. (**A** and **D**) The mean diameter ξ and (**B** and **E**) the size fluctuation χ (symbols) for (A and B) slow-moving (S) and (D and E) fast-moving (F) clusters in translational (T) and rotational (R) motions at different aspect ratios $p = a/b$. The curves are fitting functions $\xi_{F,S} = \xi_0[\phi/(\phi_{c,0} - \phi)]^{\nu}$ and $\chi_{F,S} = \chi_0[\phi/(\phi_{c,0} - \phi)]^{\gamma}$. The vertical solid and dotted lines mark the translational and rotational mode-coupling transition points $\phi_c^{T,\theta}$, above which ξ_F and χ_F decrease. The error bars denote the SDs. (**C** and **F**) ξ and χ of (C) slow and (F) fast clusters at different *p*'s (symbols) collapse onto two master fitting lines $\xi_{F,S}/\xi_0 = [\phi/(\phi_{c,0} - \phi)]^{\nu}$ and $\chi_{F,S}/\chi_0 = [\phi/(\phi_{c,0} - \phi)]^{\gamma}$. For slow clusters, ν = 1 and γ = 1.75 as in the 2D Ising universality class. Inset of (F): 1/ν and 1/γ for fast clusters increase linearly with the fragility index *D* for both translational and rotational motions. The fittings are within 5% errors.

fragility is an important question in glass studies. For example, softer particles are found to make less fragile glasses (*33*). Our fitting results show that *D* increases with *p* and is always greater than 0.6 for both translational and rotational motions of all the ellipsoids with $2.3 \leq p \leq 9$ (Fig. 2F, inset) (*30*). By contrast, $D < 0.5$ for disks with various polydispersities (*19*). Hence, even monodisperse ellipsoids are better glass formers than polydisperse spheres in 2D. This is consistent with the observation that polydisperse spheres often form crystalline patches in 2D, while ellipsoids never do. Ellipsoids under a local close packing are seldom aligned in parallel to each other because another ellipsoid can insert itself into the gap between neighboring ellipsoids and change their orientations (Fig. 1K). The bending and dendritic structures are typical constituents of quasi-nematic domains, while the splay and vortex structures are found at domain boundaries (Fig. 1K). The resulting packing configurations such as splay and bending structures have similarly high densities. These diverse close packing structures give rise to disordered solids. Hence, monodisperse ellipsoids are good glass formers with stronger frustration for higher *p*. We find that the reciprocal critical exponents 1/ν and 1/γ for the FT and FR clusters increase linearly with *D* (Fig. 2F, inset). The power-law relations of $\xi_F(\phi)$ in Fig. 2 (D to F) support the prediction of Adam-Gibbs theory that fragility (1/*D*) is a measure of the effective temperature dependence of the spatial extent of cooperative motion, i.e., the size of CRRs (*34*). A similar trend where more fragile liquids experience more pronounced growth of DHs upon cooling has been observed in the simulation of 3D binary spheres (*35*), but the linear relations in the inset of Fig. 2F have not been reported before.

The single-particle resolution enables us to measure the morphology and correlation of clusters, which can give a better understanding of the scaling universality and mechanism of critical phenomena beyond the mean-field description (*36*). The FT, FR, ST, and SR clusters all exhibit fractal structures (Fig. 1I) and the probability distribution of *N*-particle clusters $\mathcal{P}(N) \propto N^{-\mu} \exp(-N/N_0)$ (Fig. 1J) (*6*). $d_f = 1.875 \pm 0.05$ and $\mu = 2.07 \pm 0.05$ for the slow clusters (Fig. 1, I and J) coincide with $d_f = 1.875$ and $\mu = 31/15$ of the 2D Ising univerality class (*37*), but $d_f = 1.75 \pm 0.05$ and $\mu = 2.17 \pm 0.05$ for the fast clusters do not. Moreover, the hyperscaling relations for critical phenomena (*36*), $\mu = d/d_f + 1$ and $\gamma = \nu(2d_f - d)$ with the dimensionality $d = 2$, are satisfied within ±5% errors for the fast clusters near ϕ_c and for the slow clusters near ϕ_0, respectively (Figs. 1, I and J, and 2, C and F). In addition, d_f and γ/ν for the fast clusters remain almost constant at different *p*'s, while γ and *ν* vary. These features of strong universality (*36*) indicate that fast clusters in systems of different *p*'s belong to the same universality class. The higher d_f for slow clusters than for fast clusters confirms the prediction of the RFOT theory that slow CRRs are more compact than fast CRRs (*13*). A similar trend has also been observed for FT and ST clusters in the simulation of a model glass-forming polymer melt without measuring the critical behaviors (*6*).

Critical-like behaviors in structures

Critical-like behaviors of the static GT and GR clusters

We measure the mean diameter, size fluctuation, and morphology of the GT and GR clusters in the same way that we measured those of fast and slow clusters in the previous section, and similarly show

their critical-like behaviors. The mean glassy cluster diameter $\xi_G \equiv [\Sigma N_G \mathcal{P}(N_G)]^{1/d_f}$, and the fluctuations in cluster size $\chi_G \equiv \Sigma(N_G^2 \mathcal{P}(N_G))/\Sigma(N_G \mathcal{P}(N_G))$. ξ and χ can be well fitted with the 2D Ising-like power laws $\xi = \xi_0 \cdot [\phi_0^{-1}/(\phi^{-1} - \phi_0^{-1})] = \xi_0 \cdot [\phi/(\phi_0 - \phi)]$ and $\chi = \chi_0 \cdot [\phi_0^{-1}/(\phi^{-1} - \phi_0^{-1})]^{7/4} = \chi_0 \cdot [\phi/(\phi_0 - \phi)]^{7/4}$ for all aspect ratios (fig. S4). These power laws are robust when the threshold value in the criterion of glassy particles varies in [5.5,6.5] for ψ_G^T and in [0.75,0.85] for ψ_G^θ. The Ising-like criticality of glassy clusters is further confirmed by the fractal dimension d_f (Fig. 1I) and size distribution $\mathcal{P}(N) \propto N^{-\mu} \exp(-N/N_0)$ (Fig. 1J) as well as the hyperscaling relations $\mu = 2/d_f + 1$ and $\gamma = 2\nu(d_f - 1)$ with the fitted exponents $d_f = 1.875 \pm 0.05$, $\mu = 2.07 \pm 0.05$, $\nu = 1$, and $\gamma = 7/4$ (Fig. 1, I and J, and fig. S4) similar to those of slow-moving clusters.

Finite-size scaling analysis of glassy order parameter and structural entropy

The finite-size scaling (FSS) analysis is not only able to extrapolate the results of finite-sized systems to the infinite-size limit, but it is also an effective tool to ascertain critical phenomena (*38*). The FSS results for both the glassy order parameter $\psi_G^{T,\theta}$ and the structural entropy $\psi_S^{T,\theta}$ are shown in Fig. 3 for various p's and ϕ's. The spatial correlation function $C_\psi(r, L) = \langle \psi(\boldsymbol{r}_i)\psi(\boldsymbol{r}_j)\rangle_L$, where $r = |\boldsymbol{r}_i - \boldsymbol{r}_j|$ is the center-to-center separation between particles i and j from a total $N(L)$ particles in a sub-box with area $L \times L$ in the field of view. For a critical phenomenon, they should follow the 2D Ornstein-Zernike correlation function $C_\psi(r, L) \cong r^{-\eta} \exp(-r/\xi_\psi(L))$ with the Fisher critical exponent $\eta = 1/4$ (*29*, *38*). This is confirmed by the fittings in Fig. 3 (A to D). The susceptibility is defined as $\chi_\psi(L) = \langle \psi(\boldsymbol{r}_i)^2\rangle_L - \langle \psi(\boldsymbol{r}_i)\rangle_L^2$. FSS theory predicts $\xi(L, \phi) \sim L^{1/\nu} Q_\xi[L^{1/\nu}(T - T_{cri})]$ and $\chi(L, \phi) \sim L^{\gamma/\nu} Q_\xi[L^{1/\nu}(T - T_{cri})]$ (*39*), where $Q_{\xi,\chi}(x)$ are the universal scaling functions and T_{cri} is the critical temperature. These predictions are confirmed by the collapsed data in Fig. 3 (E to H) at $T_{cri} = 1/\phi_0$ with the fitted Ising critical exponents $\nu = 1$ and $\gamma = 7/4$. Moreover, the fitting exponents satisfy the Fisher scaling law $\gamma = \nu(2 - \eta)$ for critical phenomena (*29*).

A typical critical FSS behavior is that the ratios between thermodynamic quantities in the finite-size system and the infinite limit are scaling functions of $\xi(L)/L$ (*18*, *40*). Our measured ratios $\xi_\psi(L)/\xi_\psi(\infty)$ and $\chi_\psi(L)/\chi_\psi(\infty)$ as functions of $\xi_\psi(L)/L$ for various ϕ's collapse onto two master curves in the insets of Fig. 3 (E to H), whose extrapolations give $\xi(\infty)$ and $\chi(\infty)$, respectively. These curves show that the finite-size effect of $\xi(L)$ and $\chi(L)$ becomes negligible when $\xi < 0.1L$ (*39*). In addition, we find that the critical point ϕ_0 is robust to the sub-box size and agrees with the value from the VFT fitting of τ_α (fig. S2) (*30*). The extrapolated $\xi_\psi(\infty)$ (Fig. 4, A, C, D, and F) and $\chi_\psi(\infty)$ (Fig. 4, B, C, E, and F) exhibit the same Ising-like critical behaviors at ϕ_0 as those of glassy clusters (fig. S4) and slow clusters (Fig. 2, A to C) for all p's. Such consistency further lends confidence to the Ising-like criticality of glassy structures because glassy orders and structural entropies are different structural parameters without obvious connections.

The rapid growth of the structural relaxation time near the glass transition can be attributed to the growing clusters of different local structures in different systems, e.g., icosahedra, tetrahedra, and crystallites (*14*–*20*). Among them, the low-configurational-entropy clusters exist universally in different systems (*18*, *21*, *30*). The decreasing configurational entropy was originally suggested by the Adam-Gibbs theory (*2*) and further explained by the RFOT theory (*3*). However, the CRRs in these configurational-entropy pictures are not explicitly defined and demonstrated. In 2D polydisperse (*18*) and 2D binary (*18*, *21*) spherical particle systems, the faster and slower regions were observed to have higher and lower structural entropies, respectively. Tanaka *et al.* (*18*) found Ising-like power-law divergence of the correlation lengths of the local structural entropy in monolayers of binary spheres. Here, we not only find similar behaviors in monolayers of ellipsoids with different aspect ratios and both rotational and translational degrees of freedom but also further confirm the Ising-like criticality from the entropy fluctuations that have not been measured before. Such spatial and quantitative structure-dynamics

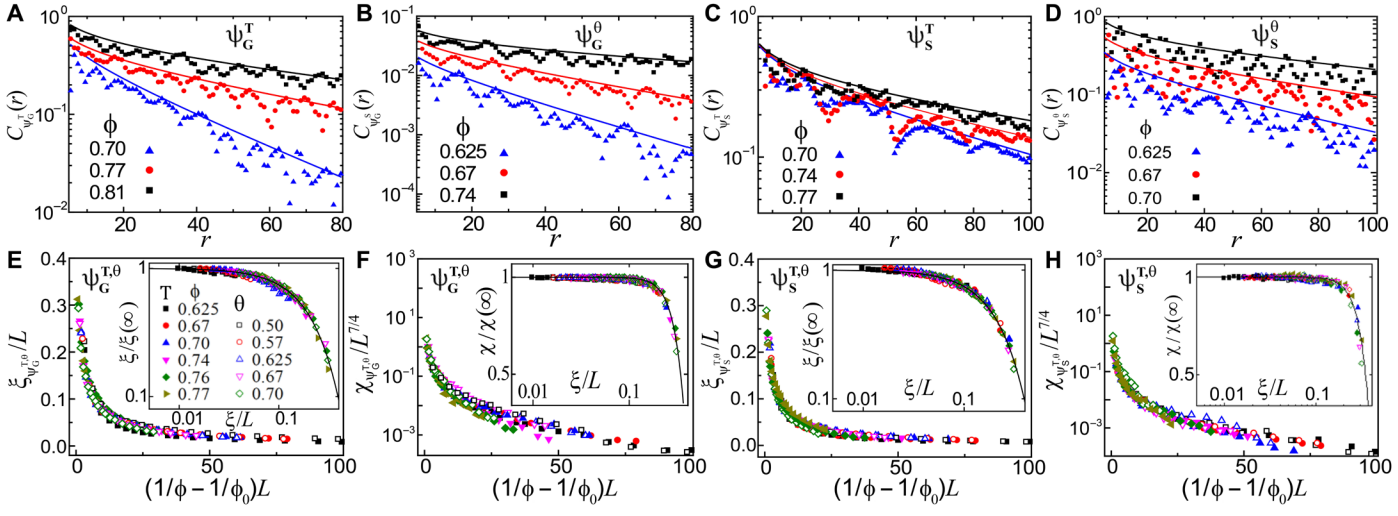

Fig. 3. FFS analyses on structures. Aspect ratio $p = a/b = 6.0$. (**A** to **D**) The spatial correlations $C_\psi(r)$ of (A) the translational and (B) orientational glassy order parameters $\psi_G^{T,\theta}$, and (C) the translational and (D) orientational structural entropies $\psi_S^{T,\theta}$. They are fitted by the 2D Ornstein-Zernike function: $C_\psi(r, L) \cong r^{-1/4} \exp(-r/\xi_\psi(L))$ (solid curves). (**E** and **G**) The fitted correlation lengths $\xi(L)$ from (A) to (D) and other ϕ's not shown in (A) to (D). (**F** and **H**) Fluctuations in ψ, i.e., $\chi(L)$. (E and F) $\psi_G^{T,\theta}$. (G and H) $\psi_S^{T,\theta}$. All the orientational data in (F) are multiplied by a factor of 88 to collapse onto the translational data. Insets: The finite-size effects of ξ and χ fitted by $\xi(L)/\xi(\infty) = \exp[-B_1(\xi(L)/L)^{B_2}]$ and $\chi(L)/\chi(\infty) = \exp[-B_3(\xi(L)/L)^{B_4}]$. B_{1-4} depends on p, but not on ϕ and the translational or rotational degree of freedom.

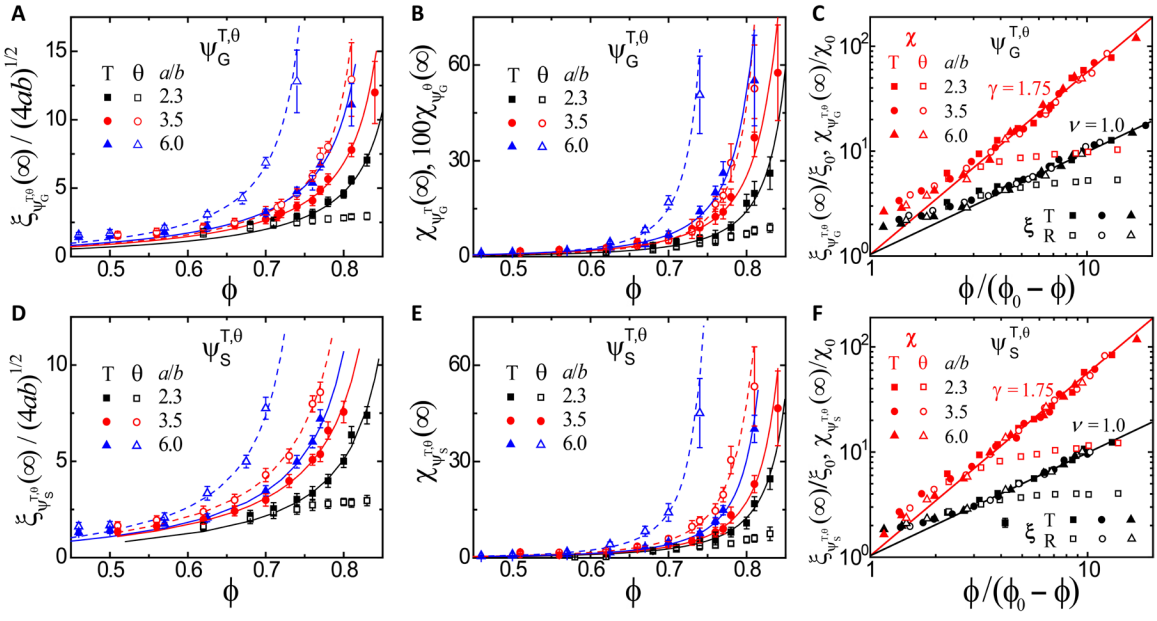

Fig. 4. Ising-like critical behaviors of structures. (**A** and **D**) The correlation length $\xi(\infty)$ (symbols) and (**B** and **E**) fluctuation $\chi(\infty)$ (symbols) of (A and B) the local glassy order parameters $\psi_G^{T,\theta}$ and (D and E) the local structural entropies $\psi_S^{T,\theta}$ at different aspect ratios $p = a/b$. The curves are fitting functions $\xi = \xi_0 \cdot [\phi/(\phi_0 - \phi)]$ and $\chi = \chi_0 \cdot [\phi/(\phi_0 - \phi)]^{7/4}$. $\xi(\infty)$ and $\chi(\infty)$ of (**C**) $\psi_G^{T,\theta}$ and (**F**) $\psi_S^{T,\theta}$ at different p's (symbols) collapse onto two master fitting lines $\xi = \xi_0 \cdot [\phi/(\phi_0 - \phi)]$ and $\chi = \chi_0 \cdot [\phi/(\phi_0 - \phi)]^{7/4}$. The fittings are within 5% errors. The deviations of $\xi_{G,S}^{\theta}$ and $\chi_{G,S}^{\theta}$ at $p = 2.3$ are due to the absence of nematic domains at small p so that the one-step glass transition is dictated by translational rather than rotational motion.

correlations in both spherical and nonspherical particle systems indicate that the structural entropy is a universal structural quantity responsible for slow dynamics.

Critical-like behaviors in temporal correlations

Temporal correlations of glassy order parameter and structural entropy

The criticality is further confirmed by the temporal correlations $S_\psi(q, t) = \langle\psi(-q,0)\psi(q, t)\rangle/[N\phi/(\pi ab)]$ (*18*) for the glassy order parameter $\psi_G^{T,\theta}$ and structural entropy $\psi_S^{T,\theta}$ (Fig. 5, A and B), where $\psi(\mathbf{q}, t) = \Sigma_{i=1}^{N} \psi_i(t) \exp(i\mathbf{q} \cdot \mathrm{r}_i)$. The behavior of $S_\psi(q, t)$ can be classified into three regimes: $q \geq 1/l$, $1/\xi \leq q < 1/l$, and $q < 1/\xi$, where $l = 2(ab)^{1/2}$ is the effective diameter of an ellipsoid and $\xi \equiv \xi_\psi(\infty)$. We find that $S_\psi(t)$ exhibits stretched exponential decay $S(q,0) \exp(-(t/\tau(q))^{\beta})$ with $\beta < 1$ at $q > 1/l$, and simple exponential decay $S(q,0) \exp(-t/\tau(q))$ (i.e., $\beta = 1$) at $q < 1/l$ (Fig. 5, A and B), where $S(q,0)$ measures the fluctuation of the glassy structure at the length scale $1/q$, and $\tau(q)$ measures the lifetime of the fluctuation (*18*). The stretched exponential decay of $S_\psi(t)$ at $q > 1/l$ reflects the heterogeneous dynamics at small length scales comparable to the particle size, i.e., the superposition of many simple exponential decays with different decay times. The single exponential decay of $S_\psi(t)$ at $q > 1/l$ indicates that the structural relaxation has become homogeneous at a length scale larger than the local structural heterogeneity. Such behavior is consistent with the purely dissipative stochastic model (kinetic Ising model) (*28*, *29*), which is also known as the time-dependent Ginzburg-Landau model (*28*), or model A in the Hohenberg and Halperin classification of critical dynamics theory (*41*).

Model A predicts a critical slowing down of the fluctuations as $\tau_\psi(\phi, q) \cong (\chi(q = 0)/L_R)[\phi/(\phi_0 - \phi)]^{\gamma}/[1 + (q\xi)^{2-\eta}]$, where L_R is the renormalized microscopic transport coefficient (*38*). At each ϕ, our measured $\tau_\psi(q)$ can be well fitted by the above prediction, $\tau \propto 1/[1 + (q\xi)^{2-\eta}]$. The fitted $\eta = 1/4$ in Fig. 5C belongs to the 2D Ising universality class (*18*). At $q < 1/\xi$, $\tau_\psi(q)$ increases very slowly as $q \to 0$ and $\tau_\psi(q = 0)$ is solely determined by ϕ (Fig. 5C). This is because the global structure at a length scale L much larger than the glassy cluster

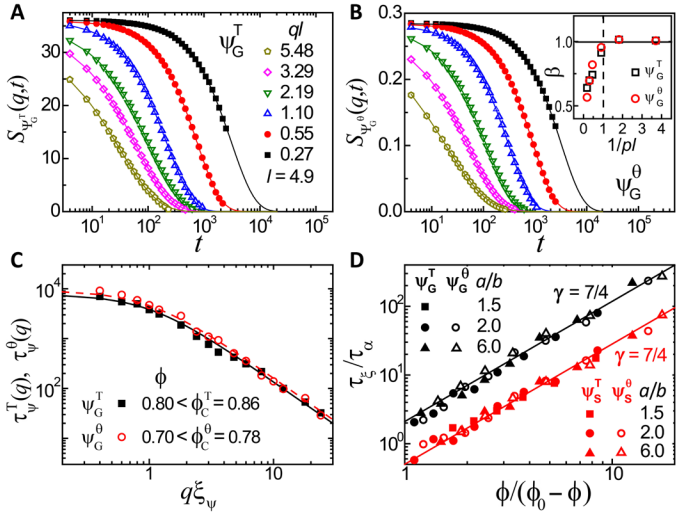

Fig. 5. Critical-like behaviors in the dynamics of structures. (**A** and **B**) The correlation function $S(q, t) = \langle\psi(q, t)\psi(-q,0)\rangle$ at different wave numbers q's for (A) the GT order parameter ψ_G^T at $\phi = 0.8$ and (B) the orientational glassy order parameter ψ_G^θ at $\phi = 0.7$. Solid fitting curves for solid symbols: $S(q, t) \sim \exp(-t/\tau(q))$. Dashed fitting curves for open symbols: $S(q, t) \sim \exp[-(t/\tau(q))^{\beta}]$ with $\beta < 1$. (**C**) The decay time $\tau(q)$ (symbols) measured from (A) and (B) fitted with $1/[1 + (q\xi)^{7/4}]$ (curves). (A to C) Aspect ratio $p = 6$. (**D**) The lifetime of structural heterogeneities of $\psi_G^{T,\theta}$ or $\psi_S^{T,\theta}$, $\tau(q = 1/\xi, \phi)$, against the structural relaxation time τ_α (symbols) at different p's are fitted with $[\phi/(\phi_0 - \phi)]^{7/4}$ (lines). The fittings are within 5% errors. Simulation data are used here because the experimental time is shorter than τ_ξ at high ϕ.

size ξ can be regarded as homogeneous, and a further increase in L does not induce additional heterogeneity or a longer decay time.

Lifetime of structural heterogeneity

In addition to the microscopic structural relaxation time τ_α on a particle length scale from the intermediate scattering function (*31*), $\tau_\xi = \tau_\psi(q = 1/\xi)$ measures the lifetime of spatial heterogeneity, i.e., how long it takes the spatial memory of high-ψ clusters to fade away. Model A predicts the power-law divergence $\tau_\xi(\phi) = \chi_0[\phi/(\phi_0 - \phi)]^\gamma/(2L_R)$, which is well confirmed by fitting $\tau_\xi/\tau_\alpha \propto [\phi/(\phi_0 - \phi)]^\gamma$ with $\gamma = 7/4$ as in the 2D Ising universality class in Fig. 5D for both glassy orders and structural entropies. $\tau_\xi \gg \tau_\alpha$ at high ϕ indicates that the structural relaxation over a length scale ξ of typical glassy clusters is a process comprising a number of microscopic relaxations at a particle length scale (*10*). The similar power laws for the structural heterogeneities and DHs indicate that τ_ξ mainly depends on the relaxation of slow-moving clusters. This result also supports the observation that the lifetime of DH is much longer than τ_α near the glass transition in fragile systems (*10*, *17*, *18*, *35*, *42*, *43*).

In fragile liquids, τ_ξ is directly related to the bulk structural and mechanical relaxation properties (*35*, *42*, *43*). The increasing τ_ξ toward ϕ_0 implies a higher resistance to stress and deformation. For example, the increasing bulk modulus near the glass transition primarily arises from the percolating slow clusters with increasing lifetimes (*44*) and the growing static length scales of orientational or amorphous order (*26*, *45*). Here, the increasing τ_ξ/τ_α toward ϕ_0 in Fig. 5D indicates that the contribution of the solid-like component related to the growing static length scale is increasing compared with the contribution of the viscous component related to the microscopic structural relaxation. This finding provides a microscopic interpretation for the sharp increase in storage modulus and the decrease in loss modulus during the glass transition (*46*).

Critical-like behaviors in simulation results

The kMC simulation results are shown in figs. S5 to S9 in section S6. These results are similar to their corresponding experimental results in Figs. 1 to 4 and fig. S4. For the one-step glass transition at $p \lesssim 1.7$ (fig. S1D), the ST and SR clusters are positively correlated with GT clusters (fig. S5, A and B) and the low translational entropy regions (fig. S5, E and F). For the two-step glass transition at $p \gtrsim 1.7$ (fig. S1D), the ST clusters are positively correlated with GT clusters (fig. S5C) and the low translational entropy regions (fig. S5G), while the SR clusters are positively correlated with orientational glassy clusters (fig. S5D) and the low orientational entropy regions (fig. S5H).

The Ising-like criticality at ϕ_0 is demonstrated by the fractal dimensions (fig. S5I), size distributions (fig. S5J), mean diameter and size fluctuations for the slow (fig. S6, A to C) and glassy (fig. S7) clusters, and the spatial correlations (fig. S8, A to D), FSS analysis (fig. S8, E to H), correlation lengths (fig. S9, A and D), and susceptibilities (fig. S9, B and E) in the infinite-size limit of the glassy order parameters (figs. S8, A, B, E, and F, and S9, A to C) and local structural entropies (figs. S8, C, D, G, and H, and S9, D to F).

The non-Ising criticality at ϕ_c is shown by the fast clusters in figs. S5 (I and J) and S6 (D to F). We find the linear relationship between fragility $1/D$ and the critical exponents ν_F and γ_F for the fast clusters (insets of fig. S6F), indicating that less anisotropic ellipsoids form a more fragile glass corresponding to a more pronounced and rapid growth of DHs upon cooling. All these simulation results confirm the experimental observations.

DISCUSSION

Summary of the main results

We have studied monolayers of monodisperse ellipsoids with different aspect ratios and analyzed four structural quantities, i.e., the translational and orientational glassy order parameters ($\psi_G^{T,\theta}$) and local structural entropies ($\psi_S^{T,\theta}$), and four dynamic quantities describing the translational and rotational fast- and slow-moving particles. On the basis of these eight quantities for individual particles, we have measured their spatial and time correlations, length scales ξ, and fluctuations χ, defined their clusters, and measured the clusters' ξ, χ, d_f, and $\mathcal{P}(N)$. These results, FSS relations, hyperscaling relations, and Fisher scaling law all demonstrate a 2D Ising-like criticality at ϕ_0 for static $\psi_G^{T,\theta}$, static $\psi_S^{T,\theta}$, static glassy clusters, and dynamic slow-moving clusters as well as a different criticality at ϕ_c for the fast-moving clusters in both translational and rotational degrees of freedom and for both single-step ($p \lesssim 2.5$) and two-step ($p \gtrsim 2.5$) glass transitions as summarized in Table 1. The finding that a glassy system with $p \gtrsim 2.5$ displays four criticalities at four densities $\phi_{c,0}^{T,\theta}$ is remarkable. The results at ϕ_0 support the Ising critical droplet model for a microscopic geometrical description of the glass transition (*36*). These rich critical-like behaviors concerning the static (high glassy orders and low structural entropies) and dynamic (slow CRRs) quantities in Table 1 provide much stronger evidence supporting the critical phenomena and thermodynamic nature of the glass transition than does the common approach of structure-dynamics correlations.

Ising-like critical behaviors at ϕ_0 were observed in various 2D and 3D glassy systems composed of spheres (*17*–*20*, *27*). The spatial and temporal correlations, results of FSS analysis, temperature dependence of lengths and fluctuations in the structural quantities, and the four-point dynamic correlation length were all found to have Ising-like critical behaviors at ϕ_0 with a strong spatial correlation between high-order structures and slow-moving regions (*17*, *18*), but the fast-moving clusters and the critical behaviors at ϕ_c have not been explored. In numerical simulations under a small shear perturbation, Ising-like critical behaviors were observed for the shear rigidity length in $NiZr_2$ metallic glasses (*24*) and for the correlation length of non-affine deformations in a binary Lennard-Jones glassy system (*23*). These studies focused on the translational degree of freedom of unary spheres with local crystalline structures (*17*–*20*) and binary spheres without obvious crystalline structures (*18*, *27*), or they did not show the corresponding type of local structure and the connection to slow dynamics (*23*, *24*). The cluster size distribution $\mathcal{P}(N) \sim N^{-\mu}$ and the fractal dimension d_f for icosahedral clusters were previously measured in polydisperse colloidal hard spheres (*17*). We find that the values do not satisfy the hyperscaling relation, consistent with the conclusion therein that icosahedral clusters are not responsible for dynamic slowdown (*17*). $\mu = 2/d_f + 1$ for polytetrahedral clusters was tested in granular hard-sphere glass (*15*), but the correlation length of polytetrahedral order diverged much faster than the Ising universality and whose quantitative connection with dynamics was not measured.

Our results introduce several new analyses for the studies of critical-like behaviors in glasses. (i) We have observed critical-like behaviors at both ϕ_c for fast-moving clusters and ϕ_0 for slow-moving and glassy clusters, which indicate a dynamic transition at ϕ_c and a thermodynamic transition at ϕ_0. (ii) The Ising-like criticality exists in non-spherical particle systems of different aspect ratios without crystalline structures, and in both translational and rotational degrees of freedom. (iii) The hyperscaling relations $\mu = d/d_f + 1$ and $\gamma = \nu(2d_f - d)$

and the fluctuations in structural entropy have not been explored in the previous studies of critical behaviors in glasses.

Absence of isotropic-nematic transition

The observed critical-like behaviors at $\phi_0^{T,\theta}$ and $\phi_c^{T,\theta}$ are not associated with the isotropic-nematic (IN) transition for the following four reasons. (i) Nematic phases have not been observed in the monodispersed ellipsoid monolayers in our experiment and simulation (*30*, *31*) and others' experiments (*47*, *48*). Both the real-space images (Fig. 1, A to H, and fig. S5, A to H) and the exponential decay in the orientational correlation functions (fig. S1F) are distinct from the algebraic decay for the quasi-long-range nematic order. Early simulations observed nematic phases in 2D ellipses because their system sizes were merely comparable to a single pseudonematic domain in our simulation and experiment; moreover, their IN transitions are at much lower area fractions than $\phi_0^{T,\theta}$ and $\phi_c^{T,\theta}$ (fig. S1C, section S2), while we did not observe the nematic phase even at those low area fractions. (ii) Ellipsoids are excellent glass formers because their curved surfaces tend to change neighbors' orientations in dense packings, which frustrates the long-range nematic order. Moreover, 2D systems have stronger long-wavelength fluctuations than those in 3D according to the Mermin-Wagner theorem and less constraints from neighboring particles, which tend to destroy long-range orders. (iii) The 2D IN transition is predicted to be a Kosterlitz-Thouless (KT) transition (*49*), which is featured with a correlation length $\sim \exp[(T - T_c)^{-1/2}]$ (*29*, *49*). By contrast, the criticality we observe belongs to the Ising universality class featured with a power-law decay of correlation length (*29*). (iv) Ellipsoids with $p \lesssim 2.5$ do not form pseudonematic domains, but they also exhibit Ising-like criticality, indicating that the criticality is irrelevant to the nematic order.

Possible origin of the Ising criticality

The Ising-like criticality of the glass transition in systems of spheres was explained by the two-state model (i.e., twofold orientational degeneracy) of locally favored structures (LFSs) (*12*, *25*, *50*). The two-state model has been used in various glass transition studies, e.g., it serves as the basis for the Anderson theory (*51*). In glass-forming systems, the LFSs, e.g., local crystalline structures or polyhedra in systems of spheres, produce medium-range correlations but frustrate the global long-range crystalline orders (*18*, *25*). Tanaka (*12*) pointed out that the renormalization of the frustration effect may change the transition from a continuous symmetry of the tensorial order parameter to a discrete Ising Z_2 symmetry due to the scalar nature of the order parameter correlation. Langer further showed that the universality of the twofold orientational degeneracy for LFS clusters in glassy systems enables them to realign in the presence of other clusters as an effective ferromagnetic interaction and gives rise to Ising-like criticality independent of the nature of ordering and the dimensionality (*25*, *50*).

The above two-state model can be similarly applied to monodisperse ellipsoids if we regard the local glassy orders or structural entropies $\psi_{G,S}^{T,\theta}$ as playing a similar role to the local crystal-like orders for spherical particles (*12*). The LFSs of ellipsoids contain splays and bending bands (Fig. 1K). They frustrate the globally favored packing of long-range nematic (crystalline) order for the rotational (translational) degree of freedom and cause the formation of locally favored glassy clusters. The neighboring glassy clusters tend to realign with each other to reduce the surface tension and structural entropy. Our results indicate that the Ising-like interaction is not only limited to the local crystalline order for the translational degree of freedom of spheres but is also applicable to the glassy structures and the structural entropy for both translational and rotational degrees of freedom of ellipsoids. The random field Ising model shows that higher disorderness may change the critical exponent of a second-order transition and change a first-order transition to second order (*52*), but its connection to the ellipsoid monolayers needs to be further explored.

Different relaxation mechanisms associated with the dynamic and structural criticalities at two time scales

Previous studies have shown that some dynamic quantities (*18*, *53*) diverge according to power laws at T_0, while other dynamic quantities diverge according to power laws at T_c (*8*, *11*, *54*). These different dynamic quantities are assumed to describe the same DHs, and thus, these observations create a mystery (*7*, *54*): "How can a dynamical correlation length diverge at two distinct temperatures?" Here, we find that this mystery can be explained if we categorize the DHs based on two types of dynamics originating from the fast-moving particles at τ_2 [e.g., the mean FT cluster size and corresponding time scale (*11*), the average mobile cluster size and string length (*8*), and the size of the unstable soft region (*54*)] and the slow-moving particles at τ_α [e.g., the mean ST and SR cluster sizes and corresponding time scales ($\sim\tau_\alpha$) (*30*), and the four-point dynamic correlation length (*18*, *53*)]. The fast- and slow-moving clusters exhibit power-law divergences at the dynamic transition point ϕ_c and the thermodynamic transition point ϕ_0, respectively. In other words, the glass dynamics cannot be adequately described by one dynamic quantity, and at least two dynamic quantities at different time scales are needed. This is reasonable because the structural relaxation in the form of CRRs occurs at different time and length scales. However, fast-moving particles are usually used to characterize DHs, a probable reason why the quantitative structure-dynamics correlations have rarely been observed.

Our findings are also consistent with predictions of thermodynamic (e.g., RFOT) theory of glass transition (*1*, *54*, *55*) that the relaxation mechanism changes from continuous diffusion above the dynamic critical transition temperature T_c to entropy-driven activated motion below T_c. This change in mechanism and the nature of T_c might be obscured by the conventionally expected single dynamic length scale (*26*). Here, our quantitative results of the fast, slow, and static glassy clusters confirm the change in mechanism across ϕ_c: The dynamic length ξ_F for fast clusters rapidly increases with τ at $\phi < \phi_c$ and diverges at ϕ_c following a power law in accordance with MCT, while the dynamic length ξ_S for slow clusters that is correlated with the static length (ξ_ψ) slowly and logarithmically increases with τ and diverges at the thermodynamic glass transition point $\phi_0 > \phi_c$, in accordance with the VFT law (*40*, *53*–*56*). In addition, in glasses composed of spheres, this change is phenomenally characterized by a change in CRRs from a ramified to a compact morphology (*13*), an increase in dynamic length above T_c with a decrease below T_c, and a continuous increase in a static correlation length (*7*, *57*). We have observed that the fast-moving particles form ramified clusters at $\phi < \phi_c$ (figs. 1, A to H, and S5, A to H). However, at $\phi_c < \phi < \phi_0$, the fast-moving particles are mainly caged, and thus, they are randomly distributed in space without forming clusters (Figs. 1D and 2, D and E, and fig. S5D). Such breakdown of fast clusters was also observed in colloidal glasses composed of spheres (*9*). By contrast, the slow particles and low-entropy glassy particles are strongly correlated in space and

form compact clusters whose mean size increases near ϕ_0 (Figs. 1, A to H, and 2, A and B, and fig. S5, A to H). Our observations provide a quantitative microscopic picture of the change in relaxation mechanism across ϕ_c: The structural relaxation is dominated by fast clusters associated with diffusion at $\phi < \phi_c$, but by glassy-structure clusters associated with low entropies at $\phi < \phi_c$. This further demonstrates that the evolution of CRRs cannot be sufficiently characterized by a unique time and length scale toward the glass transition.

Relationship between glass fragility and particle anisotropy, and the connection to universality of criticality

Besides the two criticalities at ϕ_c and ϕ_0, we have measured fragility, which is important for glassy materials. Softer particles were found to form less fragile glasses (*33*). Here, we have shown that higher particle anisotropy leads to less fragility. Moreover, fragility linearly changes with the critical exponent of fast-moving clusters. The lower fragility for more anisotropic ellipsoids reflects stronger frustrations and a higher ability to form glasses with weaker structural heterogeneities and DHs. Even ellipsoids with a modest $p = 2.3$ have a higher D than hard spheres with polydispersity up to 16% in 2D (*19*); hence, monodisperse ellipsoids are better glass formers than highly polydisperse spheres. The results are consistent with the observation that particle anisotropy can effectively frustrate crystallization, e.g., in monodisperse ellipsoids (*30*, *58*), polygon platelets (*59*), and spheres with anisotropic interactions (*20*). We attribute this to the fact that more anisotropic ellipsoids can pack into more diverse LFSs (Fig. 1K), i.e., corresponding to a more rugged energy landscape. Similarly, binary sphere mixtures (*18*, *27*) or polygon platelets (*59*) are able to pack into diverse LFSs rather than just polyhedra for polydisperse spheres and hexagon for polydisperse disks, and hence form glasses more easily.

Glassy systems with long-range ultrasoft interactions or random network structures do not exhibit DHs despite their high fragility (*60*) and, thus, may not exhibit critical behaviors. The Ising-like criticality has been found in systems of hard spheres (*17*–*19*), Lennard-Jones spheres (*18*, *20*, *23*), and our own hard ellipsoids, indicating that the critical-like behaviors tend to occur in fragile systems composed of hard-core-like particles regardless of the particle shape.

MATERIALS AND METHODS

Sample preparation and particle tracking microscopy

A 0.5-μl droplet of suspension was placed between a glass slide and a coverslip. The capillary force spread the colloidal ellipsoids into a monolayer with very weak vertical fluctuation under the strong confinement. To prevent the ellipsoids from sticking together, the glass plates were rigorously cleaned by sonication in a 1:4 mixture of hydrogen peroxide and sulfuric acid and then thoroughly rinsed in deionized water. The sample cell was sealed with epoxy glue and tilted at an angle of 5° to 30° for several hours to 1 day so that the ellipsoids slowly settled along a sample edge under gravity to form a dense monolayer. Before the measurement, the sample was placed horizontally for equilibration for 2 to 3 hours. We chose a square millimeter area in the sample with the desired area fraction ϕ and monitored an area of ~0.1 mm^2 in the center under an optical microscope for 3 to 6 hours, during which ϕ was kept constant. To change ϕ, we tilted the sample again and measured the ellipsoids in the same sample region after equilibration. The center-of-mass position and the orientation of individual ellipsoids were tracked using our image processing algorithm at spatial resolutions of 0.12 and 0.04 μm along the long and short axes, respectively, and at an angular resolution of 1° (*30*). In different quasi-2D samples with the same p, the measured mean diffusion coefficients of dilute ellipsoids are the same, which ensures the same wall separations.

Simulation

kMC simulations of the monolayer of 5000 hard ellipses were performed under the periodic boundary condition (*30*). In each kMC step, we randomly generated the translational displacements along the long axis δ_a and along the short axis δ_b, and the rotational displacement δ_θ. The displacements follow the uniform random distribution in $[-\Delta_{a,b,\theta}, \Delta_{a,b,\theta}]$ with the maximum displacements Δ satisfying $\Delta_a^2:\Delta_b^2:\Delta_\theta^2 = D_a/P(\delta_a):D_b/P(\delta_b):D_\theta/P(\delta_\theta)$, where $P(\delta_{a,b,\theta})$ are the acceptance ratios for the displacements δ_a, δ_b, and δ_θ, and $\Delta_{a,b,\theta}$ are the short-time diffusion coefficients adopted from the experiments. We tried different ratios in the simulations and further confirmed that the D of individual particles does not affect the dynamics of the system near the glass transition. The duration, Δt, of each of N_{MC} Monte Carlo steps was derived as $\Delta t/\tau_B = \Delta t D_0/b^2 = N_{MC}(1 + D_b/D_a)[\delta_a^2 p(\delta_a)/(4b^2)]$, where the Brownian time t_B is the time taken for an ellipsoid to diffuse a distance b in an infinitely dilute suspension, and $D_0 = (D_a + D_b)/2$.

SUPPLEMENTARY MATERIALS

Supplementary material for this article is available at http://advances.sciencemag.org/cgi/content/full/7/3/eabd1958/DC1

REFERENCES AND NOTES

1. L. Berthier, G. Biroli, Theoretical perspective on the glass transition and amorphous materials. *Rev. Mod. Phys.* **83**, 587–645 (2011).
2. G. Adam, J. H. Gibbs, On the temperature dependence of cooperative relaxation properties in glass-forming liquids. *J. Chem. Phys.* **43**, 139–146 (1965).
3. T. R. Kirkpatrick, D. Thirumalai, P. G. Wolynes, Scaling concepts for the dynamics of viscous liquids near an ideal glassy state. *Phys. Rev. A* **40**, 1045–1054 (1989).
4. G. Tarjus, S. A. Kivelson, Z. Nussinov, P. Viot, The frustration-based approach of supercooled liquids and the glass transition: A review and critical assessment. *J. Phys. Condens. Mat.* **17**, R1143 (2005).
5. A. C. Angell, Formation of glasses from liquids and Biopolymers. *Science* **267**, 1924–1935 (1995).
6. F. W. Starr, J. F. Douglas, S. Sastry, The relationship of dynamical heterogeneity to the Adam-Gibbs and random first-order transition theories of glass formation. *J. Chem. Phys.* **138**, 12A541 (2013).
7. W. Kob, S. Roldán-Vargas, L. Berthier, Non-monotonic temperature evolution of dynamic correlations in glass-forming liquids. *Nat. Phys.* **8**, 403–408 (2011).
8. A. S. Keys, A. R. Abate, S. C. Glotzer, D. J. Durian, Measurement of growing dynamical length scales and prediction of the jamming transition in a granular material. *Nat. Phys.* **3**, 260–264 (2007).
9. E. R. Weeks, J. C. Crocker, A. Levitt, A. Schofield, D. A. Weitz, Three-dimensional direct imaging of structural relaxation near the colloidal glass transition. *Science* **287**, 627–631 (2000).
10. M. D. Ediger, Spatially heterogeneous dynamics in supercooled liquids. *Annu. Rev. Phys. Chem.* **51**, 99–128 (2000).
11. C. Donati, S. C. Glotzer, P. H. Poole, W. Kob, S. J. Plimpton, Spatial correlations of mobility and immobility in a glass-forming Lennard-Jones liquid. *Phys. Rev. E* **60**, 3107–3119 (1999).
12. H. Tanaka, Bond orientational order in liquids: Towards a unified description of water-like anomalies, liquid-liquid transition, glass transition, and crystallization. *Eur. Phys. J. E* **35**, 113 (2012).
13. J. D. Stevenson, J. Schmalian, P. G. Wolynes, The shapes of cooperatively rearranging regions in glass-forming liquids. *Nat. Phys.* **2**, 268–274 (2006).
14. U. R. Pedersen, T. B. Schrøder, J. C. Dyre, P. Harrowell, Geometry of slow structural fluctuations in a supercooled binary alloy. *Phys. Rev. Lett.* **104**, 105701 (2010).

15. C. Xia, J. Li, Y. Cao, B. Kou, X. Xiao, K. Fezzaa, T. Xiao, Y. Wang, The structural origin of the hard-sphere glass transition in granular packing. *Nat. Commun.* **6**, 8409 (2015).
16. J. Russo, H. Tanaka, Assessing the role of static length scales behind glassy dynamics in polydisperse hard disks. *P. Natl. Acad. Sci. U.S.A.* **112**, 6920–6924 (2015).
17. M. Leocmach, H. Tanaka, Roles of icosahedral and crystal-like order in the hard spheres glass transition. *Nat. Commun.* **3**, 974 (2012).
18. H. Tanaka, T. Kawasaki, H. Shintani, K. Watanabe, Critical-like behaviour of glass-forming liquids. *Nat. Mater.* **9**, 324–331 (2010).
19. T. Kawasaki, T. Araki, H. Tanaka, Correlation between dynamic heterogeneity and medium-range order in two-dimensional glass-forming liquids. *Phys. Rev. Lett.* **99**, 215701 (2007).
20. H. Shintani, H. Tanaka, Frustration on the way to crystallization in glass. *Nat. Phys.* **2**, 200–206 (2006).
21. X. Yang, R. Liu, M. Yang, W. Wang, K. Chen, Structures of local rearrangements in soft colloidal glasses. *Phys. Rev. Lett.* **116**, 238003 (2016).
22. S. Schoenholz, E. D. Cubuk, E. Kaxiras, A. J. Liu, A structural approach to relaxation in glassy liquids. *Nat. Phys.* **12**, 469–471 (2016).
23. G. Adam, J. H. Gibbs, On the temperature dependence of cooperative relaxation properties in glasmosayebi10s-forming liquids. *J. Chem. Phys.* **43**, 139–146 (1965).
24. N. B. Weingartner, R. Soklaski, K. F. Kelton, Z. Nussinov, Dramatically growing shear rigidity length scale in the supercooled glass former NiZr. *Phys. Rev. B* **93**, 214201 (2016).
25. J. S. Langer, Theories of glass formation and the glass transition. *Rep. Prog. Phys.* **77**, 042501 (2014).
26. C. P. Royall, S. R. Williams, The role of local structure in dynamical arrest. *Phys. Rep.* **560**, 1–75 (2015).
27. H. Tong, H. Tanaka, Revealing hidden structural order controlling both fast and slow glassy dynamics in supercooled liquids. *Phys. Rev. X* **8**, 011041 (2018).
28. A. Onuki, *Phase Transition Dynamics* (Cambridge Univ. Press, 2007).
29. P. M. Chaikin, T. C. Lubensky, *Principles of Condensed Matter Physics* (Cambridge Univ. Press, 1995).
30. Z. Zheng, R. Ni, F. Wang, M. Dijkstra, Y. Wang, Y. Han, Structural signatures of dynamic heterogeneities in monolayers of colloidal ellipsoids. *Nat. Commun.* **5**, 3829 (2014).
31. Z. Zheng, F. Wang, Y. Han, Glass transitions in quasi-two-dimensional suspensions of colloidal ellipsoids. *Phys. Rev. Lett.* **107**, 65702 (2011).
32. A. Donev, I. Cisse, D. Sachs, E. A. Variano, F. H. Stillinger, R. Connelly, S. Torquato, P. M. Chaikin, Improving the density of jammed disordered packings using ellipsoids. *Science* **303**, 990–993 (2004).
33. J. Mattsson, H. M. Wyss, A. Fernandez-Nieves, K. Miyazaki, Z. Hu, D. R. Reichman, D. A. Weitz, Soft colloids make strong glasses. *Nature* **462**, 83–86 (2009).
34. F. W. Starr, J. F. Douglas, Modifying fragility and collective motion in polymer melts with nanoparticles. *Phys. Rev. Lett.* **106**, 115702 (2011).
35. K. Kim, S. Saito, Multiple length and time scales of dynamic heterogeneities in model glass-forming liquids: A systematic analysis of multi-point and multi-time correlations. *J. Chem. Phys.* **138**, 12A506 (2013).
36. A. Coniglio, A. Fierro, *Correlated Percolation in Encyclopedia of Complexity and Systems Science*, R. Meyers, Ed. (Springer, New York, 2009).
37. W. Janke, A. M. J. Schakel, Fractal structure of spin clusters and domain walls in the two-dimensional Ising model. *Phys. Rev. E* **71**, 036703 (2005).
38. D. Y. Ivanov, *Critical Behavior of Non-ideal Systems* (John Wiley & Sons, 2008).
39. P. P. Jose, D. Chakrabarti, B. Bagchi, Finite-Size Scaling in *Phase Transitions and Critical Phenomena in Phase Transitions and Critical Phenomena*, C. Domb, M. S. Green, Eds. (Academic Press, London, 1983).
40. S. Karmakar, C. Dasgupta, S. Sastry, Growing length and time scales in glass-forming liquids. *Proc. Natl. Acad. Sci. USA* **106**, 3675–3679 (2009).
41. P. C. Hohenberg, B. I. Halperin, Theory of dynamic critical phenomena. *Rev. Mod. Phys.* **49**, 435–479 (1977).
42. S. Leonard, L. Berthier, Lifetime of dynamic heterogeneity in strong and fragile kinetically constrained spin models. *J. Phys. Condens. Mat.* **17**, 45 (2005).
43. S. K. Kumar, G. Szamel, J. F. Douglas, Nature of the breakdown in the Stokes-Einstein relationship in a hard sphere fluid. *J. Chem. Phys.* **124**, 214501 (2006).
44. J. C. Conrad, P. P. Dhillon, E. R. Weeks, D. R. Reichman, D. A. Weitz, Contribution of slow clusters to the bulk elasticity near the colloidal glass transition. *Phys. Rev. Lett.* **97**, 265701 (2006).
45. M. Schlegel, J. Brujic, E. Terentjev, A. Zaccone, Local structure controls the nonaffine shear and bulk moduli of disordered solids. *Sci. Rep.* **6**, 18724 (2016).
46. J. C. Qiao, J.-M. Pelletier, Dynamic mechanical analysis in La-based bulk metallic glasses: Secondary (β) and main (α) relaxations. *J. Appl. Phys.* **112**, 083528 (2012).
47. P. J. Yunker, K. Chen, Z. Zhang, W. G. Ellenbroek, A. J. Liu, A. G. Yodh, Rotational and translational phonon modes in glasses composed of ellipsoidal particles. *Phys. Rev. E* **83**, 011403 (2011).
48. C. K. Mishra, A. Rangarajan, R. Ganapathy, Two-step glass transition induced by attractive interactions in quasi-two-dimensional suspensions of ellipsoidal particles. *Phys. Rev. Lett.* **110**, 188301 (2013).
49. R. L. C. Vink, The isotropic-to-nematic transition in a two-dimensional fluid of hard needles: A finite-size scaling study. *Eur. Phys. J. B.* **72**, 225–231 (2009).
50. J. S. Langer, Ising model of a glass transition. *Phys. Rev. E* **88**, 012122 (2013).
51. P. W. Anderson, B. I. Halperin, C. Varma, Anomalous low-temperature thermal properties of glasses and spin glasses. *Philos. Mag.* **25**, 1–9 (1972).
52. T. Nattermann, Theory of The Random Field Ising Model in *Spin Glasses and Random Fields*, A. P. Young, Ed. (World Scientific, 1998).
53. E. Flenner, H. Staley, G. Szamel, Universal features of dynamic heterogeneity in supercooled liquids. *Phys. Rev. Lett.* **112**, 097801 (2014).
54. G. Biroli, J-P. Bouchaud, The random first-order transition theory of glasses: A critical assessment. Chapter 2 in *Structural Glasses and Supercooled Liquids: Theory, Experiment, and Applications*, edited by P. G. Wolynes, V. Lubchenko (Wiley Online Library, 2012).
55. S. Franz, A. Montanari, Analytic determination of dynamical and mosaic length scales in a Kac glass model. *J. Phys. A-Math. Theor.* **40**, F251–F257 (2007).
56. C. D. Ferrier, C. Thibierge, C. Alba-Simionesco, L. Berthier, G. Biroli, J.-P. Bouchaud, F. Ladieu, D. L'Hôte, G. Tarjus, Spatial correlations in the dynamics of glassforming liquids: Experimental determination of their temperature dependence. *Phys. Rev. E* **76**, 041510 (2007).
57. K. H. Nagamanasa, S. Gokhale, A. Sood, R. Ganapathy, Direct measurements of growing amorphous order and non-monotonic dynamic correlations in a colloidal glass-former. *Nat. Phys.* **11**, 403–408 (2014).
58. W. Xu, Y. Li, Z. Sun, L. An, Hard ellipsoids: Equation of state, structure, and self-diffusion. *Phys. Rev. Lett.* **139**, 024501 (2013).
59. Y. Li, Z. Li, Z. Hou, T. Mason, K. Zhao, Z. Sun, M. Ciamarra, Dynamics in two-dimensional glassy systems of crowded Penrose kites. *Phys. Rev. Mater.* **3**, 125603 (2019).
60. G. M. Hocky, D. Coslovich, A. Ikeda, D. R. Reichman, Correlation of local order with particle mobility in supercooled liquids is highly system dependent. *Phys. Rev. Lett.* **113**, 157801 (2014).
61. Y. Han, A. M. Alsayed, M. Nobili, J. Zhang, T. C. Lubensky, A. G. Yodh, Brownian motion of an ellipsoid. *Science* **314**, 626–630 (2006).
62. Z. Zheng, Y. Han, Self-diffusion in two-dimensional hard ellipsoid suspensions. *J. Chem. Phys.* **133**, 124509 (2010).
63. R. Ni, S. Belli, R. van Roij, M. Dijkstra, Glassy dynamics, spinodal fluctuations, and the kinetic limit of nucleation in suspensions of colloidal hard rods. *Phys. Rev. Lett.* **105**, 088302 (2010).
64. N. D. Mermin, H. Wagner, Absence of ferromagnetism or antiferromagnetism in one- or two-dimensional isotropic Heisenberg models. *Phys. Rev. Lett.* **17**, 1133–1136 (1966).
65. M. A. Bates, D. Frenkel, Phase behavior of two-dimensional hard rod fluids. *J. Chem. Phys.* **112**, 10034–10041 (2000).
66. M. C. Lagomarsino, M. Dogterom, M. Dijkstra, Isotropic–nematic transition of long, thin, hard spherocylinders confined in a quasi-two-dimensional planar geometry. *J. Chem. Phys.* **119**, 35353540 (2003).
67. J. A. Cuesta, D. Frenkel, Monte Carlo simulation of two-dimensional hard ellipses. *Phys. Rev. A* **42**, 2126–2136 (1990).
68. X. Liu, H. Wang, Z. Zhang, X. Ling, Structural Origin of the Two-Step Glass Transition. *arXiv*, **1908.10538** (2019).
69. G. Delaney, D. Weaire, S. Hutzler, S. Murphy, Random packing of elliptical disks. *Phil. Mag. Lett.* **85**, 89–96 (2005).
70. R. Schilling, T. Scheidsteger, Mode coupling approach to the ideal glass transition of molecular liquids: Linear molecules. *Phys. Rev. E* **56**, 2932–2949 (1997).
71. M. Letz, R. Schilling, A. Latz, Ideal glass transitions for hard ellipsoids. *Phys. Rev. E* **62**, 5173–5178 (2000).
72. N. Lacevic, T. B. Schroder, F. W. Starr, S. C. Glotzer, Spatially heterogeneous dynamics investigated via a time-dependent four-point density correlation function. *J. Chem. Phys.* **119**, 7372–7387 (2003).
73. M. Mailman, C. F. Schreck, C. S. O'Hern, B. Chakraborty, Jamming in systems composed of frictionless ellipse-shaped particles. *Phys. Rev. Lett.* **102**, 255501 (2009).
74. R. Shekhar, J. K. Whitmer, R. Malshe, J. A. Moreno-Razo, Isotropic-nematic phase transition in the Lebwohl-Lasher model from density of states simulations. *J. Chem. Phys.* **136**, 234503 (2012).
75. A. Cuetos, M. Dijkstra, Kinetic pathways for the isotropic-nematic phase transition in a system of colloidal hard rods: A simulation study. *Phys. Rev. Lett.* **98**, 095701 (2007).
76. A. Baranyai, D. J. Evans, Direct entropy calculation from computer simulation of liquids. *Phys. Rev. A* **40**, 3817–3822 (1989).
77. D. Costa, F. Micali, F. Saija, P. V. Giaquinta, Entropy and correlations in a fluid of hard spherocylinders: The onset of nematic and smectic order. *J. Phys. Chem. B* **106**, 12297–12306 (2002).

Acknowledgments
Funding: This work was supported by the National Natural Science Foundation of China (grant nos. 11372314 and U1738118), the Strategic Priority Research Program of the Chinese Academy of Sciences (grant no. XDB22040301), the Hong Kong Research Grants Council under the General Research Fund (grant nos. 16302518 and 16301117), and the Academic Research Fund from Singapore Ministry of Education grant MOE2019-T2-2-010 and Advanced Manufacturing and Engineering Young Individual Research grant (A1784C0018).
Author contributions: Y.H., and Z.Z. designed the research. Z.Z. conducted the experiments, and R.N. conducted the simulations. Z.Z. analyzed the data. Z.Z., Y.H., and R.N wrote the manuscript. All authors reviewed the final manuscript. **Competing interests:** The authors declare that they have no competing interests. **Data and materials availability:** All data needed to evaluate the conclusions in the paper are present in the paper and/or the Supplementary Materials. Additional data related to this paper may be requested from the authors.

Submitted 6 June 2020
Accepted 20 November 2020
Published 15 January 2021
10.1126/sciadv.abd1958

Citation: Z. Zheng, R. Ni, Y. Wang, Y. Han, Translational and rotational critical-like behaviors in the glass transition of colloidal ellipsoid monolayers. *Sci. Adv.* **7**, eabd1958 (2021).